5-1-2020

Concentrating Photovoltaic Retrofit for Existing Parabolic Trough Solar Collectors: Design, Experiments, and Levelized Cost of Electricity

Todd P. Otanicar
Boise State University

Rhetta Wingert
University of Tulsa

Matthew Orosz
University of Tulsa

Clay McPheeters
SolAero Technologies Corp

Publication Information

Otanicar, Todd P.; Wingert, Rhetta; Orosz, Matthew; and McPheeters, Clay. (2020). "Concentrating Photovoltaic Retrofit for Existing Parabolic Trough Solar Collectors: Design, Experiments, and Levelized Cost of Electricity". *Applied Energy, 265*, 114751. https://doi.org/10.1016/j.apenergy.2020.114751

Concentrating Photovoltaic Retrofit for Existing Parabolic Trough Solar Collectors: Design, Experiments, and Levelized Cost of Electricity

Todd P. Otanicar*
Department of Mechanical Engineering
The University of Tulsa
Tulsa, OK, USA
and
Department of Mechanical and Biomedical Engineering
Boise State University
Boise, ID, USA
toddotanicar@boisestate.edu

Rhetta Wingert
Department of Mechanical Engineering
The University of Tulsa
Tulsa, OK, USA

Matthew Orosz
Department of Mechanical Engineering
The University of Tulsa
Tulsa, OK, USA

Clay McPheeters
SolAero Technologies Corp
Albuquerque, NM, USA

Abstract

Photovoltaics and concentrating solar thermal power are two ways for generating electricity from sunlight, albeit through different methods. Parabolic trough style powerplants represent 3.6 gigawatts of electricity production, but many of these plants are aging and being replaced with photovoltaics. An alternative option that could be employed to leverage the sunk capital cost associated with the primary optics would be the design of a pure photovoltaic retrofit working within the existing plant architecture. Here, a secondary optical concentrator is designed to use the existing primary optics of a parabolic trough type solar thermal powerplant. The design is a v-shaped secondary concentrator resulting in a predicted concentration ratio on a 20 mm wide target of 94. The concentrating photovoltaic receiver for retrofit of an RP-3 based parabolic trough has been constructed using multi-junction concentrator photovoltaic cells and experimentally demonstrated here for the first time. Calculated performance of the cells based on cell specifications should result in 31% efficiency at 85˚C. On-sun efficiencies were measured at an average value of 21% with operational temperatures between 55-120˚C. Levelized cost of electricity calculations predict the system to have the potential to be below 7¢/kWh based on predicted efficiencies and 13¢/kWh based on the measured values at cell costs of $\$5/cm^2$.

Keywords: photovoltaic (PV), concentrating solar power (CSP), solar energy, retrofit

1. Introduction

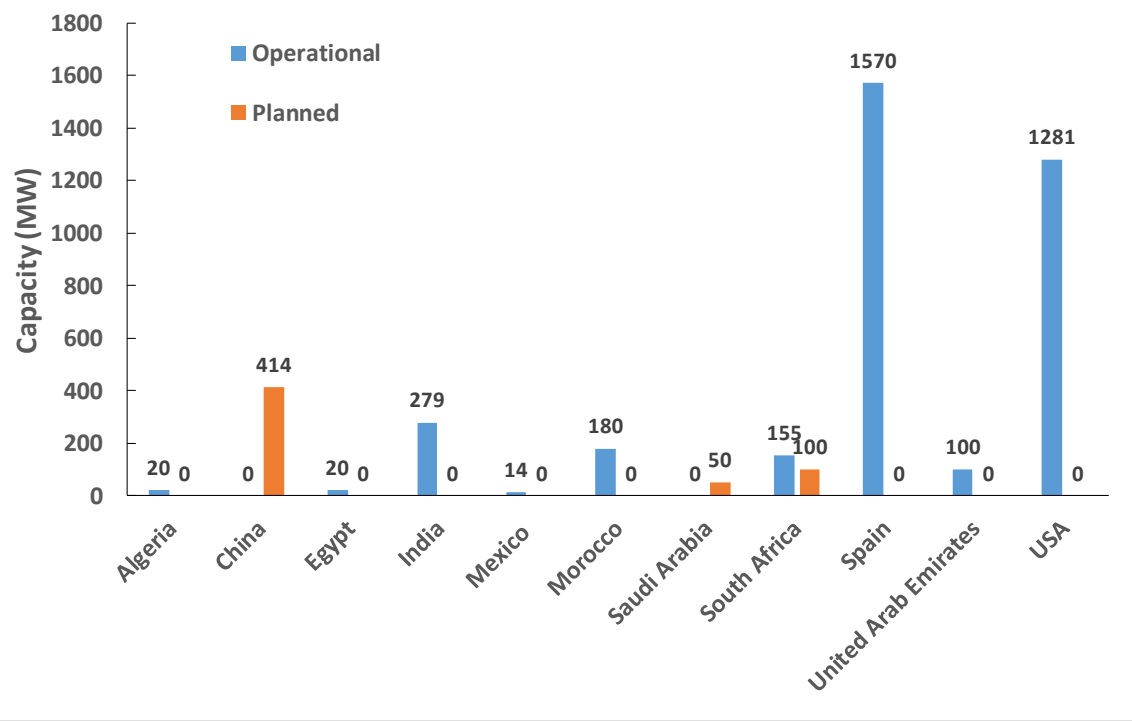

Figure 1. Total worldwide installed capacity of parabolic trough powerplants that use RP3 mirror geometry (data from SolarPACES database [1])

Generating electricity from solar energy is done through two primary pathways: photovoltaics (PV) or concentrating solar thermal power (CSP). CSP technology relies upon concentrating incoming sunlight onto a heat collection element (HCE) where it is converted to heat and then subsequently converted to electrical energy via a power cycle. CSP has extensive infrastructure worldwide, with 5498 MW of operational capacity installed, the primary advantage being the ability to store energy as heat for use later[1]. The levelized cost of electricity (LCOE) associated with CSP in 2017 was $0.22 kWh[2]. Of the total installed capacity, 3619 MW or 66% result from parabolic trough plants that utilize the Rioglass RP-3 mirror geometry as shown in Figure 1. As CSP solar collectors age, plant operators face a decision to maintain plants with rising operation and maintenance costs, replace the collectors with a different technology, or implement a retrofit to increase power output[3]. An example of this decision is the Solar Energy Generating Station (SEGS) II, a 30 MW CSP parabolic trough plant, which was decommissioned in 2014, demolished, and replaced with a 44 MW flat plate PV array with single-axis tracking[3]. As parabolic trough power plants continue to age the number of plants facing a similar fate will rise. Replacement with a PV array represents one particular form of energy conversion, but is not necessarily a useful means for utilizing a very expansive and expensive resource, i.e. the existing infrastructure of the solar field.

Global PV installation saw an increase of approximately 392 GW from 2006 to 2017, with projected growth up to 575 GW of additional infrastructure by 2023, with an LCOE of $0.05/kWh[4]. High-efficiency PV cells, such as those made using III-V semiconductors like GaAs, are often used under concentration to minimize costly cell area but suffer from problems associated with overheating[5]. The “promise” of such an approach is that the cells operate at high efficiency and expensive material usage is minimized, with the resultant potential for low levelized costs[6]. Recently, the concentrated photovoltaic (CPV) market has seen decreased global market share in comparison to 1-sun PV panels, particularly as the prices of flat plate crystalline silicon PV have dropped significantly. While the specific cost [e.g. $/W] of PV has continued to drop, there is renewed focus on applications featuring hybrid CPV and CSP.

Hybrid CSP-CPV technologies are of growing interest to simultaneously generate optimized quantities of electricity and heat. A number of systems have been proposed that use beam splitting technology, and selective spectral absorption. Orosz notably demonstrated the advantages of hybridizing photovoltaics with concentrating solar power as a means to fully utilize the full solar spectrum[7]. One design approach proposed replacing existing primary mirrors

with a "PVMirror" that is spectrally selective and includes integrated PV cells to harness the direct and diffuse components of radiation[8]. Another approach integrated highly reflective PV secondary mirror elements into the vacuum envelope of a parabolic trough heat collection element to provide additional concentration and direct PV electrical production[9]. Hybridization could also be achieved through the use of selective nanoparticle laden fluid absorbers placed in the flux line before a photovoltaic module[10]. Further interest in hybrid CSP-CPV arrangements should be directed to a recent review article highlighting a number of design configurations[5]. The vast majority of these systems utilize a parabolic trough as the primary optics for concentration. Another approach focused on a system where a dense array (DA-CPV) receiver is at the top of a central receiver cooled by R134a and coupled to an organic Rankine cycle[11]. The DA-CPV concept was also investigated for non-uniform irradiance patterns to understand the impact of module design on system performance[12]. Dish based systems have also been investigated with multi-junction and partially transmitting CPV cells to provide electrical power output and high temperature heat for industrial processes[13,14]. While hybrid systems are of growing interest, the additional equipment needed and reduction in thermal energy to the power block has limited further adoption. It remains to be seen if hybrid CPV with higher grade thermal energy will be adopted for the process heat industry where a power block isn't needed[14,15]. Additionally, a number of new CSP developments are "hybridizing" with PV to lower the LCOE of the total plant[16].

Two alternate approaches to retrofit CSP with PV involve adding PV under full spectrum in underutilized thermal receiver areas or replacing key components on CSP collectors with CPV to take advantage of the existing infrastructure. CSP fields often have spillage zones where optical errors or tracking errors result in concentrated light falling outside the focal point. Because of this wasted energy, there has been interest in integrating cells into these spillage zones. To take advantage of existing collectors, Ho et al. proposed placing PV cells in the optical spillage areas for heliostats and parabolic troughs to recover concentrated light that would otherwise be wasted[17]. In the case of parabolic trough collectors, the spillage from the troughs can cause thermal expansion in the connections between the HCEs and damage the collectors. These connections are commonly protected by finned bellows shields that cover the vulnerability and dissipate the heat. Conventional and multi-junction CPV cells placed on the underside of the bellows cover were modeled in cases of natural convection (passive) cooling, forced air convection, and forced liquid cooling[17]. At 40x concentration, the multi-junction module efficiency was approximately 25%, with forced air cooling while module efficiency for passive cooling was approximately 14%. The forced liquid cooling approach reported a module efficiency of 28% at 40 suns. Silicon cell module efficiencies for passive, forced air, and forced liquid cooling were approximately 0%, 3%, and 15%, respectively. Despite the difference in performance while on concentration, a cost analysis between the cells indicated silicon cells were more cost effective for spillage recovery for the lower irradiance zones in existing parabolic trough collector applications. Others have looked at the potential for putting PV on the drive pylons of CSP facilities[18]. While these integrations could be added at low potential LCOE, the application is limited in size due to using areas of wasted flux.

The other option is to replace components on a large scale within existing CSP facilities with PV. A number of researchers have proposed designs to substantially increase the concentration ratio of line focus concentrators (parabolic trough or linear Fresnel). Cooper et al. proposed a system that converted the line focus of a parabolic trough into a number of point foci along the axis to achieve concentration ratios in excess of 4000x[19]. Wheelwright et al. proposed a toroidal lens array that created a hyperboloid focal point with 1000x concentration[20]. It should be noted that both of these systems require complex secondary optics but are able to achieve very high concentration ratios.

Recently, lower concentration ratio approaches have been investigated as the optics and tracking are simpler and coupled with falling costs of PV cells may prove to be attractive. One approach recently investigated is the replacement of the traditional parabolic trough with a number of flat segments to focus light onto a CPV cell[21]. An experimental test confirmed good uniformity of the optics at concentration ratio approaching 8 and module level electrical efficiencies for single junction silicon solar cells of 14.3%[21]. A similar study was also conducted for a linear Fresnel design, resulting in an optical efficiency of 62%, on-sun concentration ratio of 6, and silicon solar cell module efficiencies of 13.6%[22]. Another study focused on using either a compound parabolic concentrator (CPC) or V-shaped trough as a means for low concentration line focus CPV[23]. Results indicated that a concentration ratio of 2.2 could be achieved with the V-trough but PV performance was similar to that of the CPC[23]. All of the previously mention low-concentration approaches required new primary mirrors. A simple approach to achieve a medium level of concentration without designing new primaries is that of the V-shaped trough placed near the focal point to increase the concentration (70% of the theoretical max) with a notable uniform flux on the cell[24]. This prior work optimized

the optical concept and it was proposed as a design to "salvage valuable yet cost-effective line-focus concentrator hardware"[25]. The proposed design only mentioned the optics and did not proceed with a design, build, or test of the secondary photovoltaic receiver[25].

Here we design, build, and test a secondary optical stage that can be simply integrated into an existing parabolic trough architecture. It should be noted that all of these prior approaches focused either on the optical design, system performance, and/or technoeconomic analysis of the proposal. To our knowledge this work represents the first pure CPV retrofit for existing parabolic trough geometry to be experimentally tested under realistic on-sun conditions. Here, an optical model using ray tracing is developed and confirmed with experimental testing using a photographic technique to confirm the flux distribution. A thermal and electrical model is developed to predict retrofit CPV plant performance, temperature, and LCOE. The prototype system was fabricated and installed on an experimental parabolic trough platform at The University of Tulsa and experimental testing focused on measured CPV electrical efficiency and optical performance for the proposed design.

2. Optical Modeling

The modeling effort focused on creating an optical design that could be simply integrated without additional curved mirrors, lenses, or secondary tracking as well as predicting the PV cell efficiency for the given design. Because of the desire to use a simple optical design that can be easily manufactured and installed we chose to use a previously investigated design, the Tailored Edge Ray Collector (TERC) as seen in Figure 2[24,25]. These designs have been shown to be able to achieve up to 70% of the thermodynamic limit for a line focus parabolic trough[25]. As can be seen in Fig. 2 the location of the focus for the TERC is at a location lower than the traditional focal point for the parabolic trough (z_{TERC}). The location of the offset as well as the length of the TERC secondary mirrors (l_{TERC}) is then found through ray trace optimization completed using SolTrace. Because of its prevalence in the marketplace we selected the RP-3 mirror geometry for the parabolic trough, resulting in a standard focal length of 1710 mm. Typical CSP facilities using RP-3 mirrors consist of an inner and outer mirror for a high aperture area and geometric concentration ratio. The half-aperture width of the RP-3 geometry is 3100 mm, but the primary optics are comprised of inner and outer mirrors, with the inner mirrors having a half-aperture width of 1600 mm. The assumed optical properties for the primary mirrors are: 95% reflectivity, 2.5 mrad slope

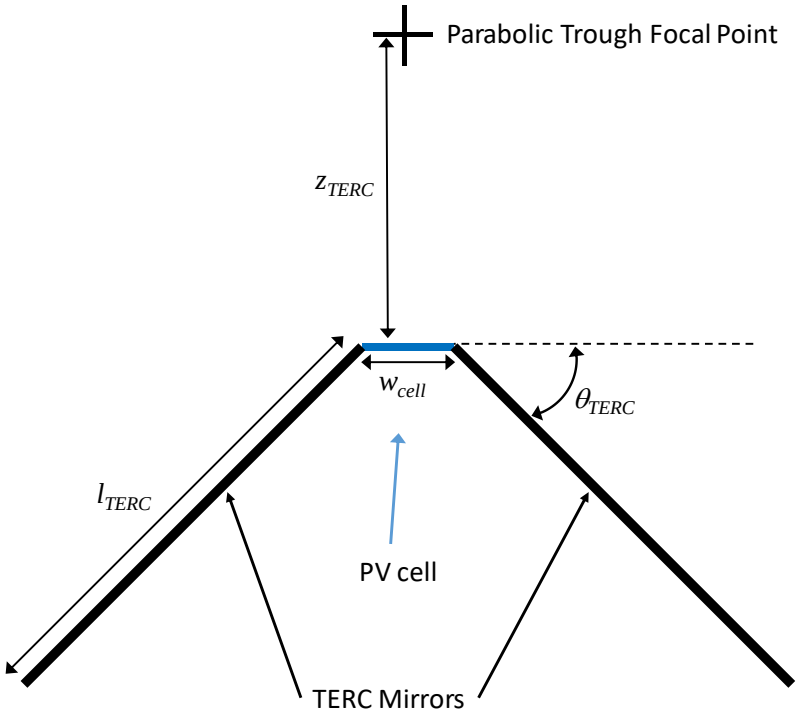

Figure 2. Simple schematic of truncated edge ray collector in parabolic trough collector

error, and 0.02 mrad specularity error. For the secondary mirrors in the TERC the reflectivity is adjusted to 90% as we chose to use Alanod Mirosun aluminum reflectors for ease of build. The model uses the optical errors and default pillbox sun shape defined in the SolTrace program. The geometric concentration ratio of the design can be found using the equation below:

$$C_{geo} = \frac{W_{mirror} - S_{TERC}}{W_{cell}} \quad (1)$$

where w_{mirror} is the width of the RP-3 mirror, s_{TERC} is the shading of the primary mirror from the TERC, and w_{cell} is the cell width.

3. Experimental Setup

The system was built and installed on an experimental parabolic trough platform located at the University of Tulsa North Campus facility, Tulsa, Oklahoma, USA (36.17 ˚N, -95.95 ˚W). The platform's primary optical system uses a standard set of inner RP-3 mirrors to concentrate the incoming light and utilizes a dual axis tracking system to reduce walk-off losses. The standard 70 mm evacuated Schott HCE was replaced with the PV retrofit and integrated into the existing fluid systems. The heat transfer fluid (HTF), Duratherm S, was circulated by a gear pump and fluid temperature at the inlet and outlet of the retrofit were measured by K-type thermocouples. Direct normal irradiance was measured with a Kipp & Zonen CHP1A pyrheliometer.

The optical system was comprised of four main elements: the aluminum substrate, TERC secondary mirrors, support ribs, and PV cells. The backbone of the retrofit was a 25.4 mm by 76.6 mm hollow rectangular aluminum substrate which supported the TERC secondary mirrors and PV

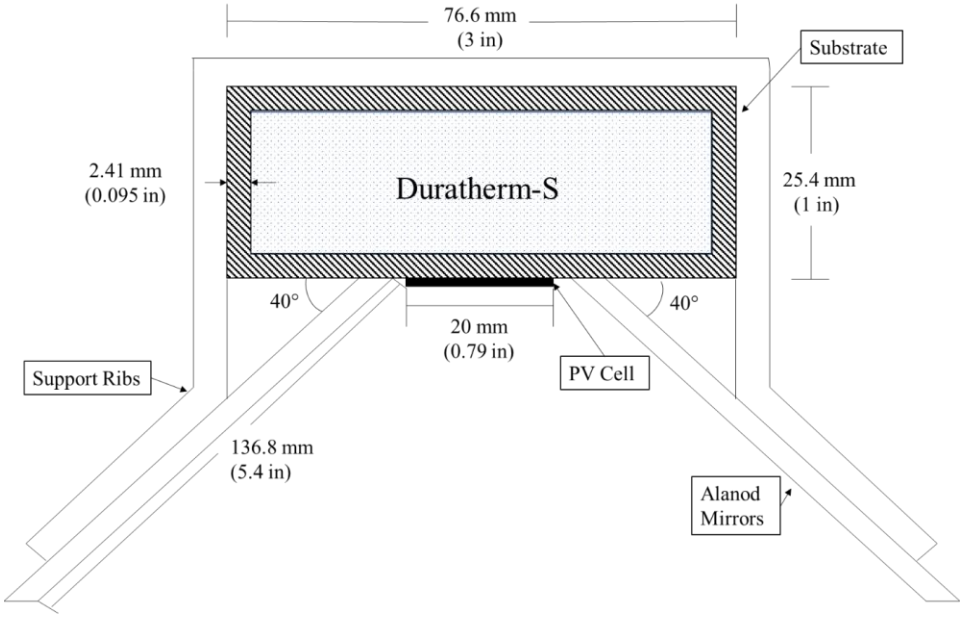

Figure 3. Cross section of TERC receiver design for inner RP-3 mirror geometry

cells, and also allowed the HTF to flow through the center and actively cool the cells. Custom inlet and outlet connectors were welded to the ends of the substrate and interface with the existing insulated stainless-steel pipes from the CSP flow loop. Figure 3 shows the retrofit cross section as designed for working on the test setup available, inner RP-3 mirrors only.

The PV cells provided by SolAero Technologies were 3rd generation triple-junction cells (ZTJ) primarily for space applications with modifications to function under concentration with an individual area of 3.68 cm^2. Notably the cells are not square and have a tapered corner, where a bypass diode is typically placed for the original usage of the cells. This area could also serve as a bypass diode location in further demonstrations and this area would be actively cooled to minimize diode heating. The provided cells have a nominal efficiency of 30.8% at 1,000 W/m^2 and 28 ˚C under

AM1.5 spectrum. Bus wires, attached to the front and back electrical contacts by hand using an ultrasonic soldering process, provided electrical leads for I-V traces while testing on sun. The PV cells were backed with a 0.5 mm thick silicone thermal pad and thermal compound paste, achieving electrical isolation and high thermal conductivity to the substrate. Typically used for cooling computer circuitry, the thermal pad and paste have a thermal conductivity of 6.0 W/m-K and 8.5 W/m-K, respectively. A section view of the substrate with the PV cells is shown in Figure 4. The cells are also protected from the elements by a thin coating of QSIL220A, a clear encapsulant. Thermocouples were buried underneath dummy cells (not used for recording electrical performance) to establish cell temperatures during concentration tests. I-V curves for individual cells were gathered at 1-sun using an Oriel Sol 1A Simulator before encapsulation. Outside 1-sun and under concentration traces were obtained using a Solmetric PVA-1000.

The black and white calibration targets between the cells allow for irradiance measurements while on concentration by the use of a photographic method developed by Sandia National Labs[26]. The targets were painted with a white reflective section the same size as the adjacent solar cells to characterize the amount of irradiance reaching a single cell. Black ends on the targets help prevent pixel saturation around the edges of the target and also provide easier identification of the “cell” edge in the target. Saturation from the secondary mirror reflection was not observed, a qualitative observation that stray rays are not being directed away from the target. The reflectance of the white reflective section on the target was measured with a Shimadzu UV-2600 UV-VIS spectrophotometer. The encapsulated targets have a calculated solar weighted reflectance of 64.56%.

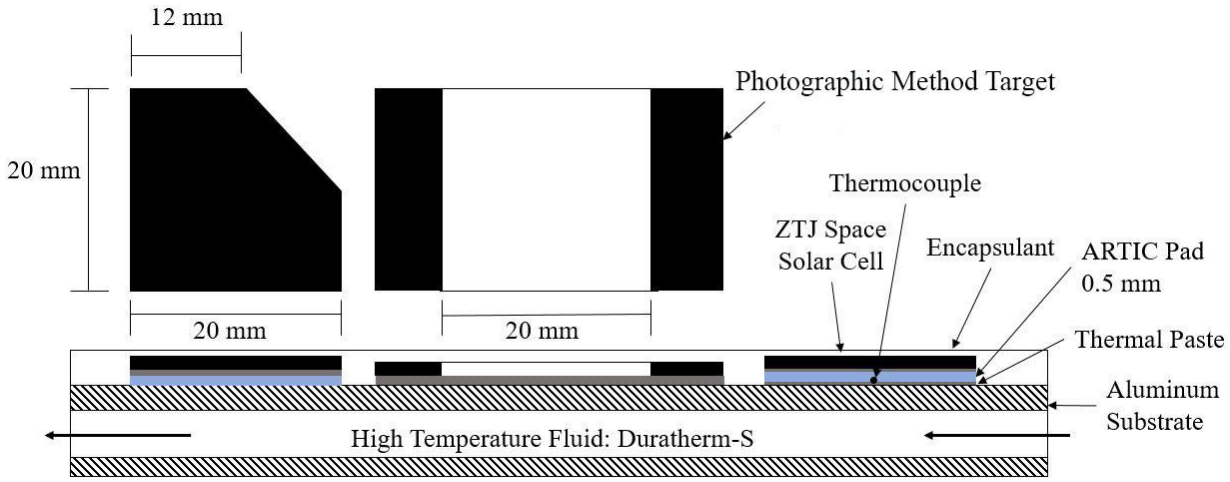

Figure 4. Top and side view of PV receiver demonstrating encapsulation layers, thermocouples and photographic flux measurement targets.

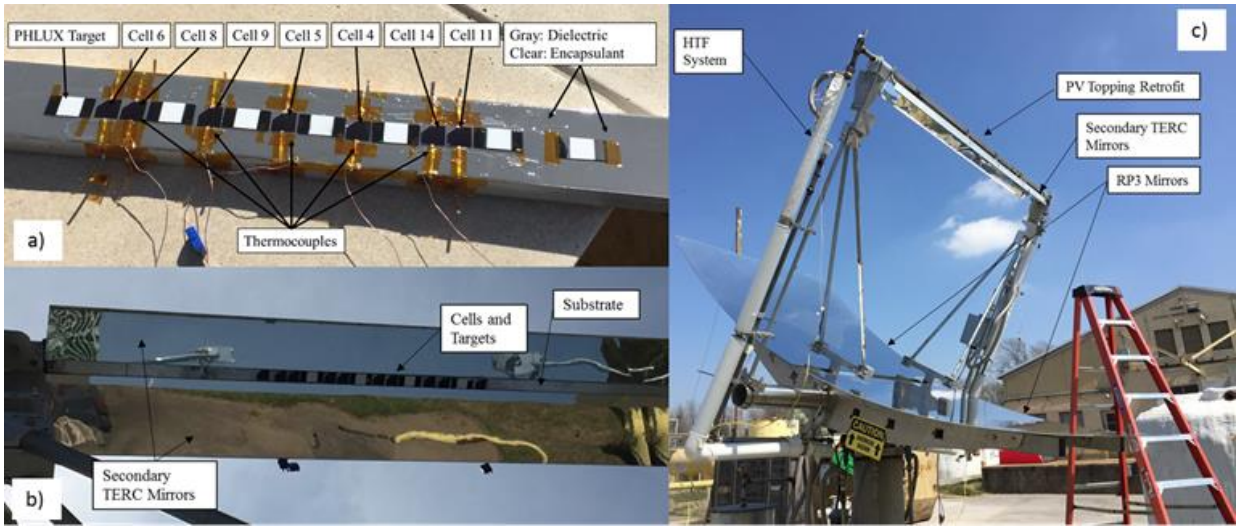

Figure 5. PV TERC Retrofit installed on parabolic trough experimental platform located at the University of Tulsa. a) Cells and PHLUX targets on receiver, b) receiver with TERC mirrors installed, and c) PV retrofit installed.

Two machined aluminum plates with tapped mounting holes and covered with a thin layer of reflective Alanod Mirosun composed the TERC mirrors. The secondary optics were attached to the substrate with machined aluminum ribs that spanned the substrate and created the 20 mm focal line for the PV cells. Each functional cell was tested for electrical continuity with the substrate and the TERC mirror to ensure electrical isolation. The HTF flowrate could not be measured while on-sun. Figure 5 shows the as-built system installed on the prototype platform.

4. Retrofit Plant Model

Simulation of the retrofit performance was performed by building a coupled thermal-electrical performance prediction model similar to prior work for hybrid CPV/T systems. The model is based upon the thermal resistance model developed for a low concentration PV/thermal system [27] and that of the miniature concentrating PV system[28]. This model was further expanded by the authors to investigate the role of the photovoltaic cell bandgap[29] and to investigate the potential hybrid system design arrangements[30]. Similar thermal models have been used recently by other authors to model the combined efficiency of spectrally selective absorbing nanofluids[31] and to model the temperature of a dense array of photovoltaics under concentration[12]. This approach simplifies the system for detailed

thermal analysis and can be coupled to predictions of cell performance provided by the manufacturer. The model is based upon the thermal resistance network outlined in Figure 6 that requires the simultaneous solution of two energy balance

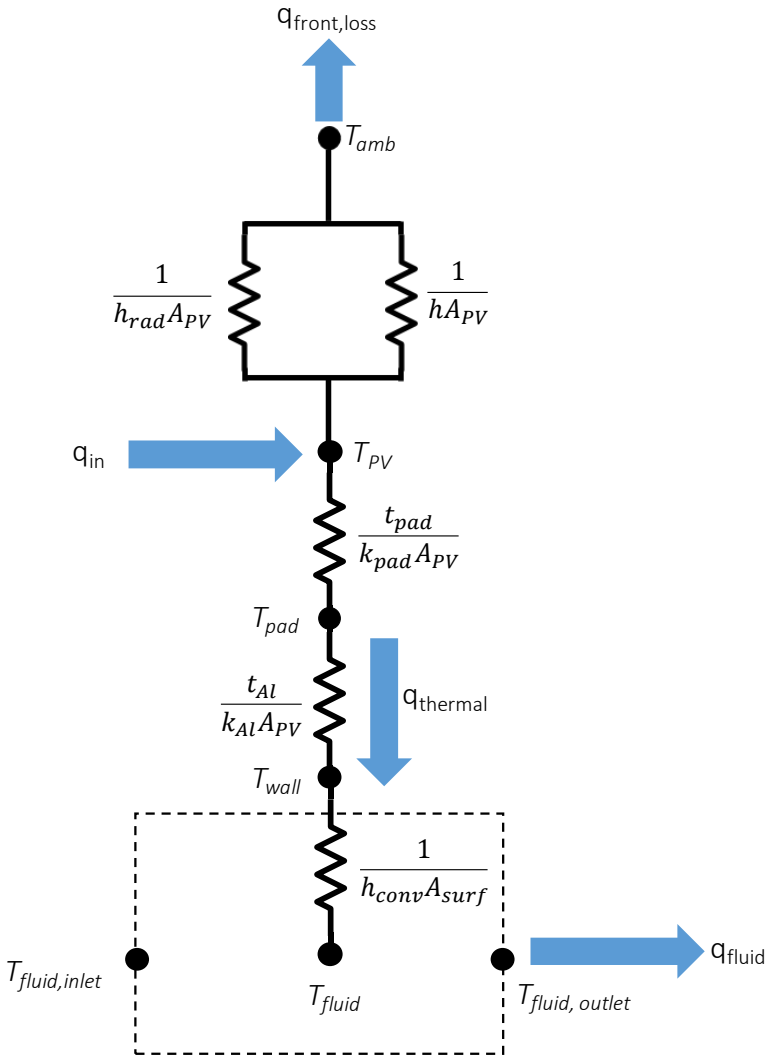

Figure 6. Thermal resistance network representation of TERC CPV receiver

equations. The back of CPV receiver is treated as adiabatic in the model, while in practice it is exposed to ambient. Not including this effect would only increase the PV temperature and therefore makes the model conservative in its estimation of PV efficiency. The model is applied along the entire length of a typical solar collector assembly (SCA) used for parabolic troughs (150 m of length) discretized to allow for solution of the spatial temperature gradient of the cooling fluid and the PV cells. The resulting energy balance equations used to solve for the temperatures of the PV cells and cooling fluid temperature are respectively:

$$q_{in} - q_{front,loss} - q_{thermal} = 0 \tag{2}$$

$$q_{thermal} - q_{fluid} = 0 \tag{3}$$

where q_{in} is the input thermal energy at the PV cell due to waste heat generation in the cell from less than 100% conversion of incoming photons to electricity, $q_{front,loss}$ is the rate of thermal energy loss from the front of the CPV receiver via both convection and radiation, $q_{thermal}$ is the thermal power transfer into the working fluid, and q_{fluid} is the thermal power in the cooling fluid. The input thermal energy at the PV cell is defined as:

$$q_{in} = \alpha GC(1 - \eta_{PV})A_{pv} \tag{4}$$

where α is the solar absorptance of the cell (assumed to be 0.90[32]), G is the input solar flux, C is the concentration ratio found during the optical modeling, A_{PV} the area of the PV cells, and η_{PV} the PV cell efficiency. The cell efficiency can be found by taking the nominal PV cell performance at 28°C under AM1.5 spectrum and estimating the performance at the expected concentration ratio using the following relationships for maximum power point voltage, current density, and efficiency respectively[33]:

$$V_{MP} = V_{MP,1-Sun} + \frac{nkT_{ref}}{q} * \ln(C) \tag{5}$$

$$J_{MP} = J_{MP,1-Sun} * C \tag{6}$$

$$\eta_{ref} = \frac{J_{MP} * V_{MP}}{G * C} \tag{7}$$

where $V_{MP,1\text{-}sun}$ is the maximum power point voltage at 1-sun AM1.5 spectrum conditions (given as 2.39 V), n the ideality factor (given as 3.4), k the Boltzmann constant, q the electron charge, T_{ref} the reference temperature (28°C), and $J_{MP,1\text{-}sun}$ is the maximum power point current density at 1-sun (given as 12.91 mA/cm^2). It should be noted that Eq. 5 is an approximation for V_{mp} and assumes changes in resistive losses in the solar cell metallization are insignificant as current changes with concentration. The impact of elevated cell temperature can be considered by modifying the resulting efficiency from equation 7 as below[34]:

$$\eta = \eta_{ref}\left[1 - \beta\left(T_{PV} - T_{ref}\right)\right] \tag{8}$$

Where η_{ref} is the reference cell efficiency, β the cell temperature coefficient (0.0023/K), and T_{PV} the cell temperature. The heat that is lost from the front of the receiver can be found from the heat transfer relationship below by considering both convection and radiation:

$$q_{front,loss} = hA_{PV}(T_{PV} - T_{amb}) + h_{rad}A_{PV}\left(T_{PV} - T_{amb}\right) \tag{9}$$

$$h_{rad} = \varepsilon\sigma(T_{PV} + T_{amb})(T_{PV}^2 + T_{amb}^2) \tag{10}$$

where h is the convection heat transfer coefficient on the CPV receiver (assumed to be 10 W/m^2-K[32]), ε is the emissivity (assumed to be 0.9[32]), σ the Stefan-Boltzmann constant, and T_{amb} the ambient temperature. The heat transferred into the fluid can be solved based on the overall thermal resistance between the PV cell and the fluid:

$$q_{thermal} = \frac{(T_{PV} - T_{fluid})}{R_{overall}} \tag{10}$$

Where T_{fluid} is the average fluid temperature from the inlet to the outlet of each section, and $R_{overall}$ is the overall thermal resistance that can be found from the following relationship:

$$R_{overall} = \frac{t_{pad}}{k_{pad}A_{PV}} + \frac{t_{Al}}{k_{Al}A_{PV}} + \frac{1}{h_{conv}A_{surf}} \tag{11}$$

Where t_{pad} is the conductive pad thickness, k_{pad} the pad thermal conductivity, t_{Al} the thickness of the aluminum wall of the CPV receiver, k_{Al} the thermal conductivity of aluminum, h_{conv} the convective heat transfer coefficient into the cooling fluid, and A_{surf} the surface area of the CPV receiver cooling channel. The convective heat transfer coefficient can be found from the Dittus-Boelter relationship when the flow is turbulent[35]. It should be noted that turbulent flow is desired to maintain low PV cell temperatures. Lastly, the energy gained by the fluid can be found:

$$q_{fluid} = \dot{m} c_p \left(T_{fluid,out} - T_{fluid,in}\right) \tag{12}$$

Where $\dot{m}$ is the mass flow rate in the CPV receiver cooling channel, c_p is the specific heat capacity of the heat transfer fluid, $T_{fluid,out}$ is the outlet fluid temperature from each section, and $T_{fluid,in}$ is the inlet fluid temperature for each section. The model is solved by sectioning an entire SCA such that the PV efficiency, PV temperature, and fluid temperature as a function of length can be determined. With the average PV efficiency over the length of one SCA the levelized cost of electricity can be estimated for the CPV retrofit[17].

$$LCOE = \frac{C_{CPV} + C_{inverter} + C_{O\&M} + C_{soft\ costs}}{E_{yearly}} * \frac{i(1+i)^n}{(1+i)^n - 1} \tag{13}$$

Where i is the interest rate (assumed to be 8%[17]), n is the number of years (taken to be 25), C_{CPV} the capital cost of the CPV retrofit, $C_{inverter}$ the inverter cost, $C_{O\&M}$ the operations and maintenance cost of the plant, $C_{soft\ costs}$ the costs associated with installation, developer cost, overhead, and sales tax, and E_{yearly} the estimated yearly energy production. The O&M cost is taken to be \$0.02/kWh based on the typical costs of O&M associated with a CSP facility[36]. The inverter and soft-costs are based on those for a typical utility scale PV facility, which is also reflective of the sunk capital from the existing CSP facility[37]. The capital cost of the CPV receiver retrofit for the current simulation is dominated by the cost of the CPV cells but the cost is estimated with the inclusion of the extrusion and the secondary mirrors.

$$C_{CPV} = C_{cell} w_{PV} L_{SCA} + C_{extrusion} L_{SCA} + C_{secondary} 2 l_{TERC} L_{SCA} \tag{14}$$

Where C_{cell} is the cell cost on a per unit area basis, w_{PV} is the width of PV cell, $C_{extrusion}$ the cost of the extrusion per unit length, $C_{secondary}$ the cost of the secondary per unit area, and L_{SCA} is the SCA length. The cost of the secondary is based on the cost of a role of aluminum and highly reflective mirror film technology, while the extrusion cost is based upon the cost of aluminum extrusion available online. The yearly energy production from the retrofit can be estimated from the following:

$$E_{yearly} = C \eta_{PV,average} A_{PV} N_{days} DNI \tag{15}$$

Where N_{days} is the number of days in a year, and DNI is the average daily flux (assumed to be 7.5 kWh/m^2-day[17]). A summary of the parameters used in the technical and economic model can be found in Table 1.

Table 1. Parameters and constants for the technical and economic model.

Parameter	Value	Units	Source
α	0.90	-	[32]
G	1000	W/m^2	Standard DNI
$V_{MP,1\text{-}sun}$	2.39	V	Assumed for multi-junction SolAero cells
n, ideality factor	3.4	-	Assumed for multi-junction SolAero cells
$J_{MP,1\text{-}sun}$	12.91	mA/cm^2	Assumed for multi-junction SolAero cells
T_{ref}	28	°C	SolAero cell data
β	0.0023	K^{-1}	SolAero cell data
h	10	W/m^2 K	[32]
ε	0.9	-	[32]
t_{pad}	0.0005	m	As built
k_{pad}	6	W/m K	Manufacturer data
t_{al}	0.00241	m	As built
k_{al}	177	W/m K	[35]
A_{surf}	29.2	m^2	As built
A_{pv}	3	m^2	As built
$\dot{m}$	3.04	kg/s	Assumed
c_p	1793	J/kg K	Duratherm S properties
$T_{fluid,in}$	30	°C	Assumed
T_{amb}	25	°C	Assumed
$C_{inverter}$	0.06	$/Wdc	[37]
$C_{O\&M}$	0.02	$/kWh	[36]
$C_{soft\ costs}$	0.41	$/Wdc	[37]
L_{sca}	150	m	Assumed
w_{PV}	0.02	m	As built
$C_{secondary}$	28	$/$m^2$	Online aluminum prices
$C_{extrusion}$	18	$/m	Online aluminum prices
C_{cell}	10000-50000	$/$m^2$	Assumed
i	8	%	[17]
n, number of years	25	Years	Assumed
DNI	7.5	kWh/m^2 day	[17]

5. Results and Discussion

5.1. Optical Results

The modeled results from SolTrace were compared to the experimental setup by using the photographic method for determining irradiance developed at Sandia National Labs, as well as through the calculation of the geometric concentration ratio. Table 2 presents a comparison of the concentration ratio obtained for both inner and inner + outer mirrors, while the experimental results are only for inner mirrors. As can be seen the geometric concentration ratio is substantially higher as it doesn't include optical losses. The estimated concentration ratio uses the optical efficiency determined within SolTrace. As can be seen the optical efficiency with the inner and outer mirrors is substantially lower than just the inners due to the wider range of incident angles on the TERC mirrors, which were designed for a system using only the inner mirrors.

Table 2. Comparison of concentration ratio based on geometry, estimation, SolTrace modeling, and experimental photographic technique.

	$C_{geometric}$	$\eta_{optical,SolTrace}$	$C_{estimate}$	$C_{SolTrace}$	$C_{photographic}$
RP-3 Inners	149	62%	93	93	74
RP-3 Inners and Outers	299	36%	108	108	-

An increase in overall concentration ratio is still achieved for the same TERC design, but further optimization using curved secondary mirrors could improve performance in a retrofit system using the inner and outer RP-3 mirrors. The photographic method from the experimental setup results in a measured concentration ratio of 74, 20% below that predicted by SolTrace but within the experimental error associated with the technique[26]. Figure 7 compares the flux profiles calculated in SolTrace with that found from the experimental method. The difference in predicted and measured flux profile is quite apparent near the outer edges of the PV cell. Experimentally a larger peak flux is observed with a narrower distribution, likely a significant amount of flux is being missed from either improper tuning of the primary mirrors or errors from assembly and build of the TERC secondary. The measured maximum irradiance using the photographic method was determined to be 100 kW/m^2, while SolTrace predicted a maximum of 87.2 kW/m^2 for the corresponding DNI of 784 W/m^2 at the time of testing. This result demonstrates decent agreement between the optical modeling and the experimentally measured irradiance at the target, but represents an area for further improvement.

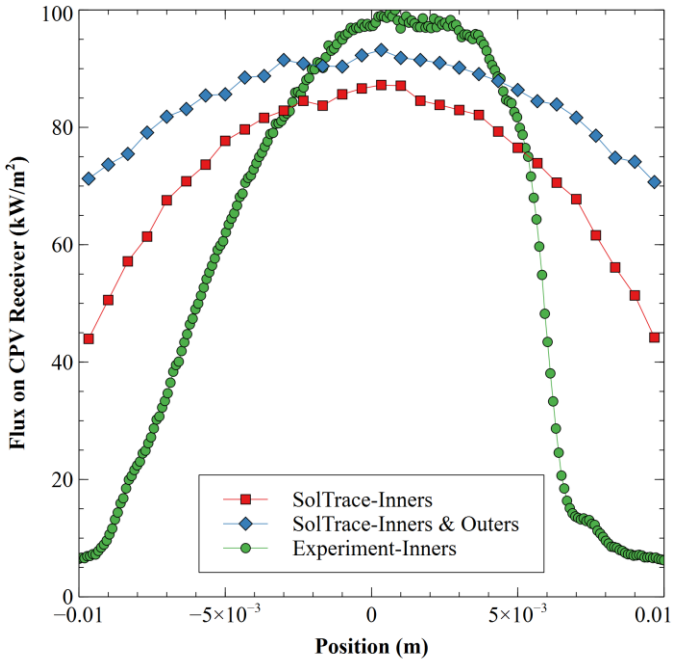

Figure 7. CPV receiver under concentrated solar flux using high ND filters for PHLUX method (top image), and calculated irradiance at target from resulting image (bottom).

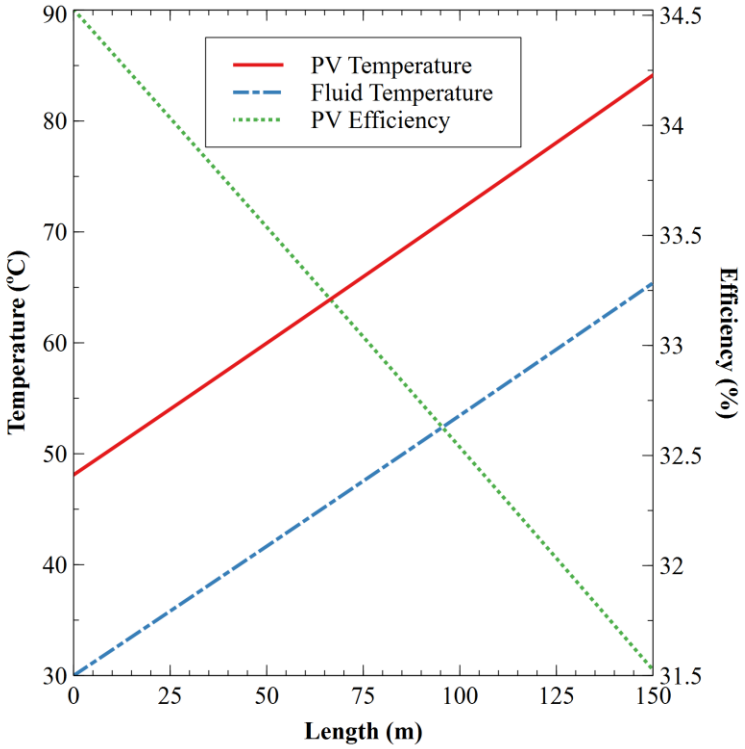

Figure 8. Predicted performance of CPV retrofit along the length of one SCA for a retrofit using both the inner and outer RP-3 mirrors of a parabolic trough (DNI=1000 W/m^2, T_{amb}=25°C, Duratherm S flow rate of 200 L/min)

5.2. Model Results

Applying the coupled thermal and electrical performance model to an SCA of length 150 m provides predictive performance results. The model uses the concentration ratio resulting from the SolTrace modeling and can be used to assess performance for a retrofit using just the inner mirrors or the inner and outer mirrors. Figure 8 displays the resulting thermal and electrical performance of the CPV retrofit for a full SCA using the inner and outer RP-3 mirrors seen in a typical parabolic trough powerplant. For the designed CPV receiver a roughly 18°C temperature difference is seen between the PV cell and the fluid temperature along the whole SCA, but it is important to note the cell temperature remains below 90°C over the whole length. The simulated PV efficiency ranges from a maximum of ~34.5% at the inlet to 31.5% at the outlet, driven by the temperature gradient along the length. Results for just the inner mirrors are similar as the concentration ratio is decreased, which lowers cell efficiency, but that effect is largely offset by the decrease in temperature from the lower concentration ratio.

5.3. Experimental Test Results

One sun indoor simulator testing was conducted on the individual ZTJ cells under a simulated AM1.5D spectrum (temperature was not controlled or measured on the simulator, but tests were conducted quickly to minimize cell heating). The testing showed an average V_{oc} of 2.659 V, an average I_{sc} of 0.043 A, and an average P_{max} of 0.098 W. The corresponding cell efficiencies (averaged of 26.8%) fell below the nominal efficiency reported in the SolAero Technologies data sheet (30.8%). Simulator data was used to identify soldered cells with cell efficiencies of 25% and above to be used in the experiment. The decrease in efficiency is likely due to the imperfect had ultrasonic soldering process, and could also be a result of simulator spectral quality (although outdoor testing produced similar results). The process is very delicate and uses special ultrasonic soldering iron equipment to hand solder the bus wire directly to the electrical contacts on the cells. It is possible that imperfect bonds created by this process reduced cell efficiency. However, pre-encapsulated cell efficiencies up to 28.5% were achieved using this method. Following encapsulation, all the cells were tested outside under non-concentrated conditions on a clear day. During the test period, the GHI was 755.5 W/m^2. Cell temperatures recorded from the dummy cells at the end of testing were 27.5° C and 25° C. Simulator and outdoor tests results, not under concentration are presented in Table 3.

Table 3. Tested cell parameters with solar simulator and outdoors without concentration

	Simulator				Outdoor "1-sun"			
Cell I.D.	**V_{oc} (V)**	**I_{sc} (A)**	**P_{max} (W)**	**Efficiency (%)**	**V_{oc} (V)**	**I_{sc} (A)**	**P_{max} (W)**	**Efficiency (%)**
31	2.65	0.043	0.100	27.2	2.59	0.040	0.092	25.0
	2.66	0.043	0.101	27.3	2.59	0.040	0.092	25.0
25	2.65	0.045	0.102	27.8	2.63	0.040	0.095	25.8
	2.68	0.044	0.102	27.6	2.63	0.039	0.094	25.5
12	2.65	0.042	0.094	25.6	2.59	0.040	0.091	24.7
	2.66	0.041	0.092	24.9	2.59	0.040	0.091	24.6
24	2.66	0.042	0.098	26.5	2.56	0.041	0.088	23.9
	2.67	0.043	0.098	26.8	2.56	0.041	0.088	23.9
32	2.65	0.043	0.099	26.9	2.60	0.040	0.094	25.5
	2.67	0.043	0.099	26.9	2.60	0.040	0.094	25.5
Average	2.66	0.043	0.099	26.8	2.6	0.040	0.092	24.9

The discrepancy between simulator and outdoor I-V traces can be attributed to the difference in irradiance, incident angle (as cells were flat but sun was not directly overhead), and encapsulant layer. After testing the cells under outdoor non-concentrating sun conditions, the secondary mirrors were attached to the retrofit. The retrofit was then installed on the prototype platform and tested under high concentration. The average V_{oc}, I_{sc}, and P_{max} were 2.741 V, 2.481 A, and 5.1 W, respectively. On-concentration produced an average 62x increase in I_{sc} when compared to the outdoor 1-sun testing which corresponds well to the measured result of the flux using the photographic method. An increase in V_{oc} when compared to 1-sun testing was on average 5%. Measured I-V curves for cell 31 can be seen in Figure 9. Cell efficiency for the experimental results is based on the measured delivered flux to the cells (the measured DNI times the measured concentration ratio, C=74).

The average cell efficiency while under concentration is 21.3% with the highest at 25.4% for cell 31 at a temperature of 80° C. Measurements for on concentration with the TERC design are documented in Table 3. Maximum temperatures were recorded at the end of each I-V measurement to determine the highest temperature observed at the dummy cell. While the CPV receiver had active cooling, it was not possible at the time to measure the flow rate. This limitation does not allow for direct comparison of the model output temperatures to the measured temperatures here.

Because rapid heating of the cells and fluid was observed it is likely that the pump was not providing enough pressure for turbulent flow, due to the high viscosity associated with Duratherm S at these temperatures. Modeling confirmed that at laminar flow rates the PV cell temperatures would exceed temperatures of greater than 200°C, raising concern about operation of the system due to maximum temperature limitations of the Duratherm S (under air), and the silicon encapsulant used. This resulted in putting the receiver on-sun, taking measurements, and then

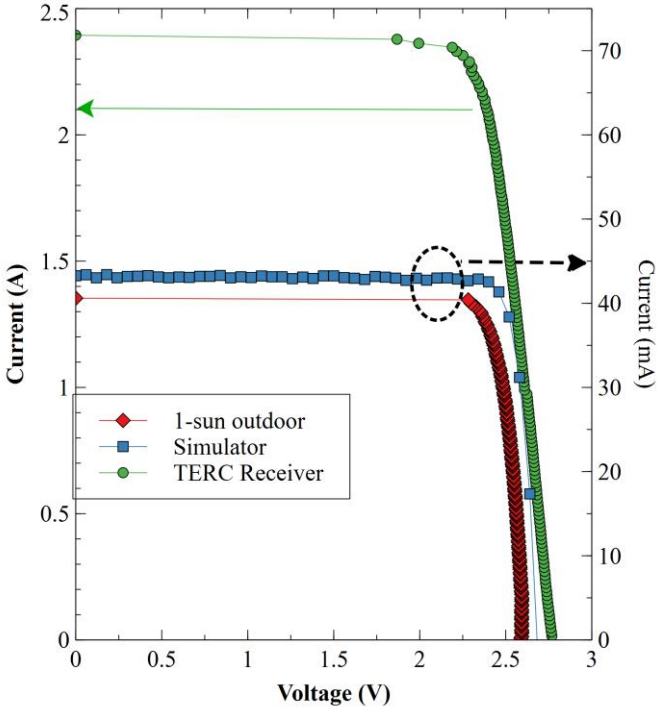

Fig. 9. Measured I-V curves of Cell 31 using solar simulator (right vertical axis), outdoor 1-sun testing (right vertical axis), and concentrated TERC CPV receiver (left vertical axis)

removing the receiver from the sun to ensure no damage to the system resulted. Per the modeling results, a flow rate of 200 L/min for the CPV receiver geometry used results in turbulent flow would limit temperatures of the PV elements to under 90°C for up to 150 m of SCA length. Table 4 also indicates differences based on time of day of operation. Experiments were run over 2 days (March 17th and March 26th), with tests on the 17th being later in the afternoon and tests on the 26th being within 25 minutes of solar noon (12:39 PM). As can be seen tests on the 26th generally had higher efficiency (22.0% vs. 20.6%) despite operating at lower DNI (871 vs. 890 W/m^2) and higher temperatures (89.4°C vs. 84°C). This difference is likely due to errors associated with tracking the sun, the primary mirror alignment, and/or differences in the alignment of the 2 TERC mirrors on the CPV receiver. This is also confirmed by the variation in measured I_{sc} over a given test period.

In order to estimate expected performance under concentration, data provided from SolAero in conjunction with equations 5-8 is used based on the concentration ratio from SolTrace modeling and the measured temperatures seen during the experimental testing. The expected performance and a comparison of all the experiments and projected performance levels is shown in Table 5. The model results assume the temperature observed in experimental testing and concentration ratio observed in the experimental campaign.

As can be seen in Table 5 the TERC performance experimentally measured is significantly lower than that of the predicted system. Potential reasons for this could be non-uniform cell irradiance, non-uniform cell temperatures, as well as poor electrical connections resulting in degraded performance at higher current. Photographic measurements of the flux revealed significant variations in the flux from the center of the cells to the outer edges that could degrade cell performance. The temperature gradient is likely small due to the small size of the cells. The electrical connections are likely to be a large source of performance loss (observed at 1-sun relative to the datasheet) and due to the difficulty of achieving solid electrical contact via hand soldering which would be exacerbated at high current.

Table 4. Experimentally measured cell performance of Solaero ZTJ cells incorporated into TERC CPV receiver integrated as part of RP3 retrofit (NR – Not Recorded)

Cell I.D.	V_{oc} (V)	I_{sc} (A)	P_{max} (W)	Efficiency (%)	DNI (W/m^2)	Dummy Cell Temperature (^{0}C)	Date	Time
31	2.80	1.72	4.21	17.0	909	NR	3/17/2019	1:33 PM
	2.78	2.39	5.24	21.2	907	NR	3/17/2019	1:58 PM
	3.00	3.00	6.11	25.4	884	80	3/17/2019	2:37 PM
	2.81	1.85	4.14	17.6	864	57	3/26/2019	12:18 PM
	2.77	1.84	4.33	18.3	870	68	3/26/2019	12:19 PM
25	2.79	1.78	4.28	18.3	857	NR	3/17/2019	1:34 PM
	2.79	2.34	5.13	22.3	844	NR	3/17/2019	1:59 PM
	2.78	2.49	5.26	21.9	881	NR	3/17/2019	2:39 PM
	2.71	2.78	5.89	24.8	873	NR	3/26/2019	12:21 PM
	2.67	2.71	5.79	24.5	867	NR	3/26/2019	12:22 PM
12	2.78	2.54	5.51	22.3	909	90	3/17/2019	1:37 PM
	2.72	2.43	5.07	20.6	903	84	3/17/2019	2:01 PM
	2.77	2.29	4.81	20.1	879	NR	3/17/2019	2:40 PM
	2.74	2.20	4.83	20.5	864	77	3/26/2019	12:25 PM
	2.71	2.71	4.89	20.4	879	81	3/26/2019	12:27 PM
24	2.75	2.50	4.88	19.6	912	NR	3/17/2019	1:49 PM
	2.80	2.66	5.10	20.8	902	75	3/17/2019	2:05 PM
	2.79	2.52	4.65	19.4	881	86	3/17/2019	2:41 PM
	2.79	2.30	4.28	17.8	883	86	3/17/2019	2:44 PM
	2.69	2.82	5.47	22.8	880	89	3/26/2019	12:29 PM
	2.66	2.87	5.50	23.1	875	96	3/26/2019	12:31 PM
	2.71	2.41	4.83	20.3	873	84	3/26/2019	12:38 PM
	2.58	2.88	5.26	22.2	869	110	3/26/2019	12:41 PM
32	2.83	2.36	4.88	19.7	909	NR	3/17/2019	1:52 PM
	2.80	2.65	5.36	21.8	901	83	3/17/2019	1:55 PM
	2.76	2.62	5.27	21.9	883	88	3/17/2019	2:07 PM
	2.65	2.77	5.78	24.3	874	94	3/26/2019	2:43 PM
	2.61	2.81	5.76	24.2	873	101	3/26/2019	12:34 PM
	2.63	2.37	4.91	20.7	873	97	3/26/2019	12:35 PM
	2.52	2.86	5.60	23.6	871	119	3/26/2019	12:39 PM
Average	2.74	2.48	5.10	21.3	882	87.3		

Table 5. Comparison of experimentally measured performance

	Simulator	Outdoor "1-Sun"	TERC Retrofit	Model for Inners
V_{oc} (V)	2.66	2.59	2.74	-
I_{sc} (A)	0.043	0.04	2.48	-
P_{max} (W)	0.098	0.092	5.10	-
Efficiency (%)	26.8	25.0	21.3	31.2

Using the results of both the experimental campaign and performance model it is possible to predict the potential LCOE that could be achieved using a TERC retrofit. The predicted LCOE assumes that all of the existing capital cost is tied to the original project and the cost of the retrofit is driven exclusively by the cell cost. Based on this assumption the results are displayed in Table 6. Using both the inner and outer mirrors results in an LCOE, assuming GaAs-based CPV cell cost of \$5/cm^2, that is just above the 2020 Sunshot goal that was achieved in 2017 of 6¢/kWh[38]. With reductions in cell cost the LCOE could achieve the Sunshot 2030 targets (<3¢/kWh) based on the model predictions[38]. Based on the experimental results the projected LCOE is 12.9¢/kWh, in line with current utility scale

PV costs. The work completed here represents another avenue to increase the value and extend the life of existing CSP facilities by retrofitting them for pure PV output. The design is based upon the most prevalent primary mirror optical geometry in the CSP industry while using available multi-junction CPV cells.

Table 6. LCOE for different assumed cell costs, modeled and experimentally measured efficiencies.

			LCOE ($/kWh)		
	Average PV Temperature (^oC)	Average PV Efficiency (%)	Cell Cost ($5/cm^2)	Cell Cost ($2.5/cm^2)	Cell Cost ($1/cm^2)
Model for Inners & Outers	66	33%	0.067	0.043	0.029
Model for Inners	61	33%	0.075	0.047	0.030
Experimental Results (inners only)	86	21%	0.129	0.075	0.042

6. Conclusion

This project successfully demonstrated an all photovoltaic retrofit on existing parabolic geometry (inner RP-3 mirrors only) to generate power from photovoltaic cells with a maximum measured cell efficiency of 25.4% based on flux delivered to the cells. As noted, this represents the first experimental demonstration in on-sun conditions of a pure concentrating photovoltaic retrofit to be applied to existing concentrating solar thermal power plants. The work completed represents a relatively simple way to preserve the existing infrastructure in the solar field while creating a means to produce electricity at low levelized costs. The photographic method independently verified the maximum irradiance delivered to the cells as predicted for the SolTrace model, also confirmed by the relative increase in short circuit current. Using the designed receiver, the cells reached an average cell efficiency of 21%, which is below the predicted cell efficiency at 74x concentration and 85° C. This decreased efficiency is likely due to the decreased starting efficiency at 1 sun and the non-uniform flux line delivered to the cells that was observed during experimental testing. Modeling predicts the potential of a retrofit concentrating photovoltaic system to produce power at an average cell efficiency of 33% (based on flux delivered) and levelized costs of electricity of less than 7¢/kWh when the full RP-3 trough is utilized. Based on the experimental results observed here, the levelized cost of electricity is 12.9¢/kWh at cell costs of $5/cm^2. If cell costs can approach $1/cm^2 the levelized cost of electricity predicted from the modeling effort falls below the U.S. Department of Energy SunShot 2030 levelized cost of electricity target of 3¢/kWh. In conclusion, the secondary mirror configuration shows promise as a viable design to generate electricity with a photovoltaic retrofit on pre-existing parabolic trough collectors, and the results of this first-generation prototype represent a potential pathway for leveraging existing infrastructure for low levelized cost of electricity concentrating photovoltaics. Future work to further develop the concept should focus on:

- Full optimization of the secondary by investigating the potential for curved secondary mirrors while balancing the cost. Increasing the optical efficiency of the design has the potential to reduce the levelized cost of electricity for higher cell costs.
- Construction of secondary mirrors with more precision to ensure uniform flux line across the cells.
- Assessment of system performance for differing photovoltaic cell materials and types.
- Characterization of thermal performance on-sun, with detailed flowrate measurements.

Acknowledgment

The authors would like to acknowledge the support provided by the U.S. Department of Energy ARPAE-FOCUS award number DE-AR0000508.

References

[1] National Renewable Energy Laboratory. Concentrating Solar Power Projects - Parabolic Trough Projects | Concentrating Solar Power | NREL 2017. https://www.nrel.gov/csp/solarpaces/parabolic_trough.cfm.

[2] Kost C, Schlegl T, Thomsen J, Nold S, Mayer J. Levelized Cost of Electricity: Renewable Energies. 2012.

[3] O'Hern H, Orosz M, Otanicar T. Parabolic trough powerplants nearing PPA end: Retrofit or replace? SolarPACES 2017, vol. 2033, 2018, p. 030010. https://doi.org/10.1063/1.5067026.

[4] Fu R, Feldman DJ, Margolis RM. U.S. Solar Photovoltaic System Cost Benchmark: Q1 2018. Golden, CO (United States): 2018. https://doi.org/10.2172/1483475.

[5] Ju X, Xu C, Hu Y, Han X, Wei G, Du X. A review on the development of photovoltaic/concentrated solar power (PV-CSP) hybrid systems. Sol Energy Mater Sol Cells 2017;161:305–27. https://doi.org/10.1016/j.solmat.2016.12.004.

[6] Swanson RM. The promise of concentrators. Prog Photovoltaics Res Appl 2000;8:93–111. https://doi.org/10.1002/(SICI)1099-159X(200001/02)8:1<93::AID-PIP303>3.0.CO;2-S.

[7] Orosz M. Photovoltaics and concentrating solar power : why hybridization makes sense. SPIE Newsroom 2015:1–4. https://doi.org/10.1117/2.1201508.006018.

[8] Yu ZJ, Fisher KC, Wheelwright BM, Angel RP, Holman ZC. PVMirror: A New Concept for Tandem Solar Cells and Hybrid Solar Converters. IEEE J Photovoltaics 2015:1–9. https://doi.org/10.1109/JPHOTOV.2015.2458571.

[9] Winston R, Yablonovitch E, Jiang L, Widyolar BK, Abdelhamid M, Scranton G, et al. Hybrid solar collector using nonimaging optics and photovoltaic components. Proc SPIE 9572 2015;9572:957208. https://doi.org/10.1117/12.2191943.

[10] Otanicar T, Dale J, Orosz M, Brekke N, DeJarnette D, Tunkara E, et al. Experimental evaluation of a prototype hybrid CPV/T system utilizing a nanoparticle fluid absorber at elevated temperatures. Appl Energy 2018;228:1531–9. https://doi.org/10.1016/j.apenergy.2018.07.055.

[11] Han X, Zhao G, Xu C, Ju X, Du X, Yang Y. Parametric analysis of a hybrid solar concentrating photovoltaic/concentrating solar power (CPV/CSP) system. Appl Energy 2017;189:520–33. https://doi.org/10.1016/j.apenergy.2016.12.049.

[12] Ju X, Pan X, Zhang Z, Xu C, Wei G. Thermal and electrical performance of the dense-array concentrating photovoltaic (DA-CPV) system under non-uniform illumination. Appl Energy 2019;250:904–15. https://doi.org/10.1016/j.apenergy.2019.05.083.

[13] Xu Q, Ji Y, Riggs B, Ollanik A, Farrar-Foley N, Ermer JH, et al. A transmissive, spectrum-splitting concentrating photovoltaic module for hybrid photovoltaic-solar thermal energy conversion. Sol Energy 2016;137:585–93. https://doi.org/10.1016/j.solener.2016.08.057.

[14] Robertson J, Riggs B, Islam K, Ji YV, Spitler CM, Gupta N, et al. Field testing of a spectrum-splitting transmissive concentrator photovoltaic module. Renew Energy 2019;139:806–14. https://doi.org/10.1016/j.renene.2019.02.117.

[15] Widyolar B, Jiang L, Winston R. Spectral beam splitting in hybrid PV/T parabolic trough systems for power generation. Appl Energy 2018;209:236–50. https://doi.org/10.1016/j.apenergy.2017.10.078.

[16] Green A, Diep C, Dunn R, Dent J. High Capacity Factor CSP-PV Hybrid Systems. Energy Procedia 2015;69:2049–59. https://doi.org/10.1016/j.egypro.2015.03.218.

[17] Ho CK, McPheeters CO, Sharps PR. Hybrid CSP/PV receivers: Converting optical spillage to electricity. AIP Conf Proc 2018;2033. https://doi.org/10.1063/1.5067170.

[18] Kurup P, Turchi C, Horowitz K, Merrigan T. SolAero Technologies Final Report: Investigation of the Potential Integration of High-Temperature Concentrator Photovoltaics and Concentrated Solar Power, and Possible Routes to Commercialization. 2017.

[19] Cooper T, Ambrosetti G, Pedretti A, Steinfeld A. Theory and design of line-to-point focus solar concentrators with tracking secondary optics. Appl Opt 2013;52:8586–616. https://doi.org/10.1364/AO.52.008586.

[20] Wheelwright BM, Angel R, Coughenour B. Freeform lens design to achieve 1000X solar concentration with a parabolic trough reflector. Proc SPIE - Int Soc Opt Eng 2014;9293:929316. https://doi.org/10.1117/12.2076091.

[21] Wang G, Wang F, Chen Z, Hu P, Cao R. Experimental study and optical analyses of a multi-segment plate (MSP) concentrator for solar concentration photovoltaic (CPV) system. Renew Energy 2019;134:284–91. https://doi.org/10.1016/j.renene.2018.11.009.

[22] Wang G, Wang F, Shen F, Jiang T, Chen Z, Hu P. Experimental and optical performances of a solar CPV device using a linear Fresnel reflector concentrator. Renew Energy 2020;146:2351–61. https://doi.org/10.1016/j.renene.2019.08.090.

[23] Singh H, Sabry M, Redpath DAG. Experimental investigations into low concentrating line axis solar concentrators for CPV applications. Sol Energy 2016;136:421–7. https://doi.org/10.1016/j.solener.2016.07.029.

[24] Friedman RP, Gordon JM, Ries H. Compact high-flux two-stage solar collectors based on tailored edge-ray concentrators. Sol Energy 1996;56:607–15. https://doi.org/10.1016/0038-092X(96)00015-1.

[25] Gordon JM. A 100-sun linear photovoltaic solar concentrator design from inexpensive commercial components. Sol Energy 1996;57:301–5. https://doi.org/10.1016/S0038-092X(96)00102-8.

[26] Ho CK, Khalsa SS. A Photographic Flux Mapping Method for Concentrating Solar Collectors and Receivers. J Sol Energy Eng 2012;134:041004. https://doi.org/10.1115/1.4006892.

[27] Rosell JI, Vallverdú X, Lechón M a., Ibáñez M. Design and simulation of a low concentrating photovoltaic/thermal system. Energy Convers Manag 2005;46:3034–46. https://doi.org/10.1016/j.enconman.2005.01.012.

[28] Kribus A, Kaftori D, Mittelman G, Hirshfeld A, Flitsanov Y, Dayan A. A miniature concentrating photovoltaic and thermal system. Energy Convers Manag 2006;47:3582–90. https://doi.org/10.1016/j.enconman.2006.01.013.

[29] Otanicar T, Chowdhury I, Phelan PE, Prasher R. Parametric analysis of a coupled photovoltaic/thermal concentrating solar collector for electricity generation. J Appl Phys 2010;108:114907. https://doi.org/10.1063/1.3514590.

[30] Otanicar TP, Theisen S, Norman T, Tyagi H, Taylor R a. Envisioning advanced solar electricity generation: Parametric studies of CPV/T systems with spectral filtering and high temperature PV. Appl Energy 2015;140:224–33. https://doi.org/10.1016/j.apenergy.2014.11.073.

[31] Crisostomo F, Hjerrild N, Mesgari S, Li Q, Taylor RA. A hybrid PV/T collector using spectrally selective absorbing nanofluids. Appl Energy 2017;193:1–14. https://doi.org/10.1016/j.apenergy.2017.02.028.

[32] Otanicar TP, Chowdhury I, Prasher R, Phelan PE. Band-Gap Tuned Direct Absorption for a Hybrid Concentrating Solar Photovoltaic/Thermal System. J Sol Energy Eng 2011;133:041014. https://doi.org/10.1115/1.4004708.

[33] Markvart T. Solar Electricity. 2nd ed. John Wiley & Sons, Ltd; 2009.

[34] Skoplaki E, Palyvos JA. On the temperature dependence of photovoltaic module electrical performance: A review of efficiency/power correlations. Sol Energy 2009;83:614–24. https://doi.org/10.1016/j.solener.2008.10.008.

[35] Bergman TL, Lavine AS. Fundamentals of Heat and Mass Transfer. 8th ed. Wiley; 2019.

[36] IRENA. Renewable Energy Technologies: Cost Analysis Series: Concentrating Solar Power. vol. 1. 2012.

[37] Fu R, Feldman DJ, Margolis RM. U.S. Solar Photovoltaic System Cost Benchmark: Q1 2018. 2018. https://doi.org/10.2172/1483475.

[38] The SunShot Initiative's 2030 Goal: 3¢ per Kilowatt Hour for Solar Electricity. 2016.